

Modulation of electrical and optical properties of gallium-doped ZnO films by radio frequency magnetron sputtering*

Liang Shuang(梁爽), Mei Zeng-Xia(梅增霞)[†], and Du Xiao-Long(杜小龙)

*Beijing National Laboratory for Condensed Matter Physics, Institute of Physics,
Chinese Academy of Sciences, Beijing 100190, China*

(Received 21 December 2011; revised manuscript received 10 February 2012)

Ga-doped ZnO (GZO) films are prepared on amorphous glass substrates at room temperature by radio frequency magnetron sputtering. The results reveal that the gallium doping efficiency, which will have an important influence on the electrical and optical properties of the film, can be governed greatly by the deposition pressure and film thickness. The position shifts of the ZnO (002) peaks in X-ray diffraction (XRD) measurements and the varied Hall mobility and carrier concentration confirms this result. The low Hall mobility is attributed to the grain boundary barrier scattering. The estimated height of barrier decreases with the increase of carrier concentration, and the trapping state density is nearly constant. According to defect formation energies and relevant chemical reactions, the photoluminescence (PL) peaks at 2.46 eV and 3.07 eV are attributed to oxygen vacancies and zinc vacancies, respectively. The substitution of more Ga atoms for Zn vacancies with the increase in film thickness is also confirmed by the PL spectrum. The obvious blueshift of the optical bandgap with an increase of carrier concentration is explained well by the Burstein–Moss (BM) effect. The bandgap difference between 3.18 eV and 3.37 eV, about 0.2 eV, is attributed to the metal–semiconductor transition.

Keywords: doping efficiency, Hall mobility, photoluminescence, Burstein–Moss effect

PACS: 73.61.Ga, 78.55.Et, 72.10.Fk, 81.15.Cd **DOI:** 10.1088/1674-1056/21/6/067306

1. Introduction

Transparent conducting oxides (TCOs) have attracted extensive attention due to their versatile applications such as light emitting diodes, random access memories, low-emissivity windows, and transparent electrodes for solar cells or flat panel displays.^[1–4] ZnO, a promising alternative to the high cost and scarce TCO (In₂O₃:Sn), has been investigated due to its benign nature, low cost, direct bandgap of about 3.37 eV, and large work function.^[5–7] To realize the higher conductivity, transparency, and stability, various dopants have been introduced to prepare the high-quality n- or p-type ZnO films.^[8–11] In fact, some aspects must be considered as follows:^[12–15] the mismatch dopants that cause interstitial donors or the host lattice relaxation, solubility limit, strengths of complex bonds, surface segregations of dopants, and self-compensating effects from native defects. In theory, Group III elements such as In, Al, and Ga

can be n-type doping candidates by substituting Zn in a ZnO host lattice. Among them, Ga is considered as the best dopant due to its nearly ionic radius and its oxidation resistance ability. Therefore, a variety of techniques have been used such as magnetron sputtering,^[16] pulsed laser deposition,^[17] chemical vapour deposition,^[18] and spray pyrolysis.^[19] Magnetron sputtering is widely used for fabricating TCOs due to easy control, high efficiency, and economy. Although many research findings have been reported for the doped ZnO films, the discrepancies still exist. Currently, most electrical resistivity results reported are in a range of 10^{−4} Ω·cm in magnitude. However, the measured Hall mobility can vary several times, even in the films having a similar carrier or doping concentration.^[20] The photoluminescence (PL) spectra also show some controversies,^[21,22] which are a convenient method to detect radiative defects in materials. In spite of the variations in the values reported by different authors, there might be a correla-

*Project supported by the National Natural Science Foundation of China (Grant Nos. 61076007 and 11174348), the National Basic Research Program of China (Grant Nos. 2009CB929404 and 2011CB302002), and the Knowledge Innovation Project of the Chinese Academy of Sciences.

[†]Corresponding author. E-mail: zxmei@aphy.iphy.ac.cn

© 2012 Chinese Physical Society and IOP Publishing Ltd

<http://iopscience.iop.org/cpb> <http://cpb.iphy.ac.cn>

tion between deposition parameters and properties of the films. In fact, it has been suggested that the deposition parameter can also have an important influence on composition homogeneity, defect chemistry, and crystal microstructure of the film.^[23,24] In the present work, some deposition parameters and physical mechanisms are investigated to clarify some controllable factors of the optical and electrical behaviours for the doped ZnO films.

In this study, we chose Ga as the dopant and the Ga-doped ZnO (GZO) films are prepared at room temperature. The lower deposition temperature will extend the application fields of the TCOs. The structure, the electrical and optical data of the ZnO films are analysed to clarify some controllable factors within the properties of the films with deposition parameters such as the deposition pressure and film thickness. Our results show that the doping efficiency, the grain boundary barrier, the status of defects, and the optical bandgap can be modulated significantly by the growth process.

2. Experiment

GZO films were grown on glass substrates at room temperature by radio frequency magnetron sputtering. Two thickness ranges of 80 nm–720 nm and 60 nm–580 nm were obtained at the sputtering pressures of 0.6 Pa and 4 Pa, respectively. The sintered ceramic target, which is made from ZnO (99.995% purity) and 3 wt% Ga₂O₃ (99.999% purity), was used. The size of the target was 2 inch in diameter. The base pressure of the chamber was kept below 2×10^{-4} Pa by a turbomolecular pump. The substrate was kept at 300 K in the growth process. Argon gas was introduced as the working gas, and the argon gas flow rate was 20 SCCM (SCCM stands for cubic centimeter per minute at standard temperature and pressure). The sputtering power was kept at 80 W.

To analyse the properties of the films, film thicknesses were measured by a profilometer. Crystal structure was examined by an X-ray diffractometer (XRD) with a Cu K_{α1} radiation of 0.154 nm. A scanning electron microscope (SEM) with a field emission gun was adopted to characterize the film surface morphology. Electrical properties were measured by a Hall measuring system using the Van Der Pauw technique. Ohmic contacts were achieved by soldering small dots of indium onto the four corners of 10 mm × 10 mm film. The optical transmittance was evaluated by a

UV-visible spectrophotometer. Low temperature PL spectra at 77 K were obtained by using the 325-nm line of an He–Cd laser with a power density of $1 \text{ W} \cdot \text{cm}^{-2}$.

3. Results and discussion

Figures 1(a) and 1(b) show the XRD patterns of the films in the semilogarithmic scale. The films with thicknesses of 80 nm–480 nm are prepared at 0.6 Pa, and the films with thicknesses of 60 nm–580 nm are prepared at 4 Pa. The absence of the segregated phase excludes the possibility of large-size precipitates in the films. However, it is very difficult for the XRD to detect nanosized clusters and precipitates around grain boundaries. Both figures show that the diffraction intensity of the ZnO (002) peak increases and becomes dominant with the increase of film thickness. It indicates that the films are highly textured along the *c* axis. However, other peaks emerge weakly. The films grown at 0.6 Pa show relatively clear ZnO (101) and (103) peaks. During the film growth, the deposition pressure can change the growth mode and the film quality, which are associated with the preferential nucleation, sticking probability, and surface diffusion. In fact, the preferential orientation of polycrystalline films and associated morphologies and properties are central topics for film growth. The relationship between growth conditions and the preferential orientation has been confirmed.^[25] As shown in the figures, the (002) face is more dominant at a higher sputtering pressure of 4 Pa due to the lowest surface energy growth mode. It is also observed that the position of the ZnO (002) peak shifts toward the higher angle with the increase of film thickness, regardless of preparation conditions. The peak position shift of the (002) orientation was also reported by Hong *et al.*,^[26] but it is the result of the post-annealing treatment. The peak position shifts toward the higher angle side from 33.8° to 34.16° at the sputtering pressure of 0.6 Pa, and from 34° to 34.22° at the sputtering pressure of 4 Pa. The full width at the half maximum (FWHM) value decreases with the increase of film thickness. This should be attributed mostly to the relaxed lattice strain and improved film quality, which consequently favours the substitution of more Ga atoms for Zn atoms in the ZnO host lattice. In other words, the Ga_{Zn} concentration will be enhanced with the increase in film thickness as confirmed by the electrical measurements.

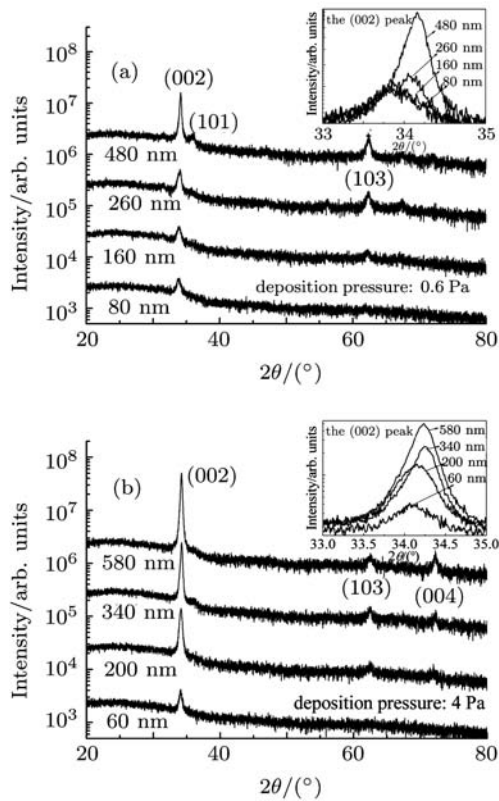


Fig. 1. The XRD patterns of the GZO films with different thicknesses. In panel (a), the thicknesses of 80, 160, 260, and 480 nm are obtained at 0.6 Pa; in panel (b), the thicknesses of 60, 200, 340, and 580 nm are obtained at 4 Pa. The inserts show the position shifts of (002) peaks.

The SEM images, which are given in Fig. 2, show the influence of the film thickness and the deposition pressure on the surface morphology. In the initial period, the film thicknesses are 80 nm and 60 nm, and the small crystallites are around 30 nm–40 nm in diameter. The small crystallites are the origin of the broadened diffraction peaks. As film thickness increases, the grains begin to coalesce. However, the grain shapes and surface morphologies are different for the films deposited at 0.6 Pa and 4 Pa. The films deposited at 0.6 Pa have more irregular morphologies. This should be attributed to the different growth modes, which arise from the different growth rates and aggregation rates of the emerging crystal faces.^[27] This is in accordance with XRD measurements. It is believed that in the initial period, the randomly oriented nucleation will occur due to the amorphous glass substrate. However, the deposition pressure can change the preferential nucleation, the (002) preferential nucleation will be more dominant at 4 Pa, but the (101) and (103) orientations can survive weakly at 0.6 Pa. The difference between the morphologies, due to the different growth rates and

aggregation rates of different crystal faces, becomes more and more clear. Moreover, different surface morphologies lead to a considerable difference in electrical properties.

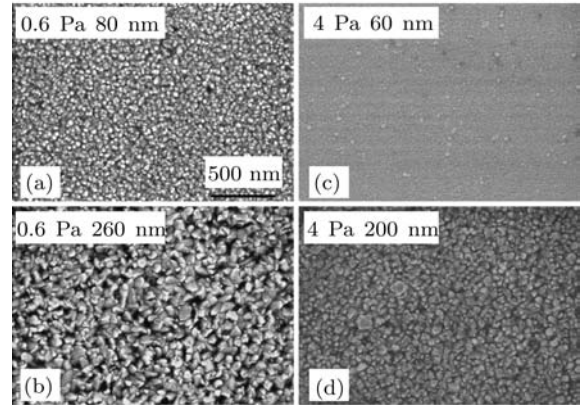


Fig. 2. SEM images of films with different thicknesses, the films in panels (a) and (b) are prepared at 0.6 Pa and have thicknesses of 80 nm and 260 nm respectively; the films in panels (c) and (d) are prepared at 4 Pa and have thicknesses of 60 nm and 200 nm respectively.

The dependences of the electrical resistivity on the film thickness are shown in Fig. 3(a). As seen, the electrical resistivity increases rapidly with the decrease of film thickness. It should be noted that the electrical resistivity ρ of the film with a thickness of 60 nm, prepared at 4 Pa, is $\sim 1.67 \times 10^{-2} \Omega \cdot \text{cm}$. This is attributed to the deactivation of Ga dopants due to the higher deposition pressure.^[28] Figure 3(b) shows the resistivity, carrier concentration, and Hall mobility, each as a function of film thickness. The films with thicknesses of 80 nm to 720 nm are prepared at 0.6 Pa. A similar trend is also observed for the films prepared at 4 Pa, but not shown here. The resistivity decreases with the increase of film thickness. This results from the increase in both carrier concentration and Hall mobility. As shown in the figure, n_c and μ_c can be modulated in ranges of $\sim 2.1 \times 10^{20} \text{ cm}^{-3}$ – $4.3 \times 10^{20} \text{ cm}^{-3}$ and $\sim 6.7 \text{ cm}^2 \cdot \text{V}^{-1} \cdot \text{s}^{-1}$ – $13.3 \text{ cm}^2 \cdot \text{V}^{-1} \cdot \text{s}^{-1}$ by the film thickness respectively. It is believed that the obvious improvement arises from more Ga atoms having been substituted for Zn atoms, which leads to a higher quality of film. The result is consistent with that shown by the regular position shifts of the ZnO (002) peaks in XRD measurements. Actually, it is not desirable for TCO to have too high a carrier concentration ($n_c > 10^{21} \text{ cm}^{-3}$), which can have a strong absorption effect in the near infrared region and will reduce the wide optical bandpass needed. From this viewpoint, the mobility plays a more important role. The

current challenges are how to enhance the carrier mobility and how to find the main obstacles which affect the mobility. Figure 3(c) sorts all the present data in a plot of the Hall mobility versus the carrier concentration. The films with various carrier concentrations are prepared at 0.6 Pa and 4 Pa, respectively. As demonstrated above, the modulation of carrier concentration from $1.09 \times 10^{20} \text{ cm}^{-3}$ up to $5.17 \times 10^{20} \text{ cm}^{-3}$ can be achieved by adjusting the deposition pressure and the film thickness. The top-right data point with n_c of $\sim 5.17 \times 10^{20} \text{ cm}^{-3}$ and μ_c of $\sim 16.1 \text{ cm}^2 \cdot \text{V}^{-1} \cdot \text{s}^{-1}$ represents the lowest resistivity ρ , $\sim 7.5 \times 10^{-4} \Omega \cdot \text{cm}$. The figure also shows the upper limit of the semi-empirical model developed by Masetti *et al.*^[29] In this model the ionized impurity scattering and impurity cluster scattering effects are taken into consideration, which can be described as

$$\begin{aligned} \mu_{\text{in}} &= \mu_{\text{Ma}} \\ &= \mu_{\text{min}} + \frac{\mu_{\text{max}} - \mu_{\text{min}}}{1 + (n/n_{\text{ref1}})} - \frac{\mu_1}{1 + (n_{\text{ref2}}/n)^2} \end{aligned} \quad (1)$$

with $\mu_{\text{max}} = 210 \text{ cm}^2 \cdot \text{V}^{-1} \cdot \text{s}^{-1}$, $\mu_{\text{min}} = 50 \text{ cm}^2 \cdot \text{V}^{-1} \cdot \text{s}^{-1}$, $\mu_1 = 40 \text{ cm}^2 \cdot \text{V}^{-1} \cdot \text{s}^{-1}$, $n_{\text{ref1}} = 2 \times 10^{18} \text{ cm}^{-3}$, and $n_{\text{ref2}} = 6 \times 10^{20} \text{ cm}^{-3}$,^[7] μ_{in} has been estimated (the fitted curve in Fig. 3(c)). As is known, for heavily doped oxide films ($n_c > 10^{20} \text{ cm}^{-3}$), the

ionized impurity scattering should be predominant and the trend of mobility will be inverse to that of carrier concentration. However, our results show that the mobility is enhanced with the increase of carrier concentration. The results suggest that the grain boundary scattering is abundant in the film.^[7,30,31] In fact, it is also observed that the resistivity can fluctuate slightly and randomly as soon as the film is exposed to a high humid environment. This finding was also reported by Tadatsugu.^[30] Usually, the grain boundary has remarkable effects on the properties of materials such as strength,^[32] ferroelectric property,^[33] and magnetic property.^[34] The grain boundary consists of the disordered atom layers, impurities of dielectric mismatch, and absorbed gas such as O_2 , which can capture excess electrons from the conduction band and can cause an upward band bending around grain boundaries. The grain boundary scattering model was proposed by John.^[35] In the model there are considered trapping states located between the Fermi energy and the intrinsic Fermi energy and the limiting of the electrical transport in the polycrystalline material. The model can be expressed as

$$\mu_c = \mu_{\text{in}} \exp(-\Phi_b/kT), \quad (2)$$

$$\Phi_b = e^2 N_{\text{T}}^2 / 8\epsilon\epsilon_0 n_c, \quad (3)$$

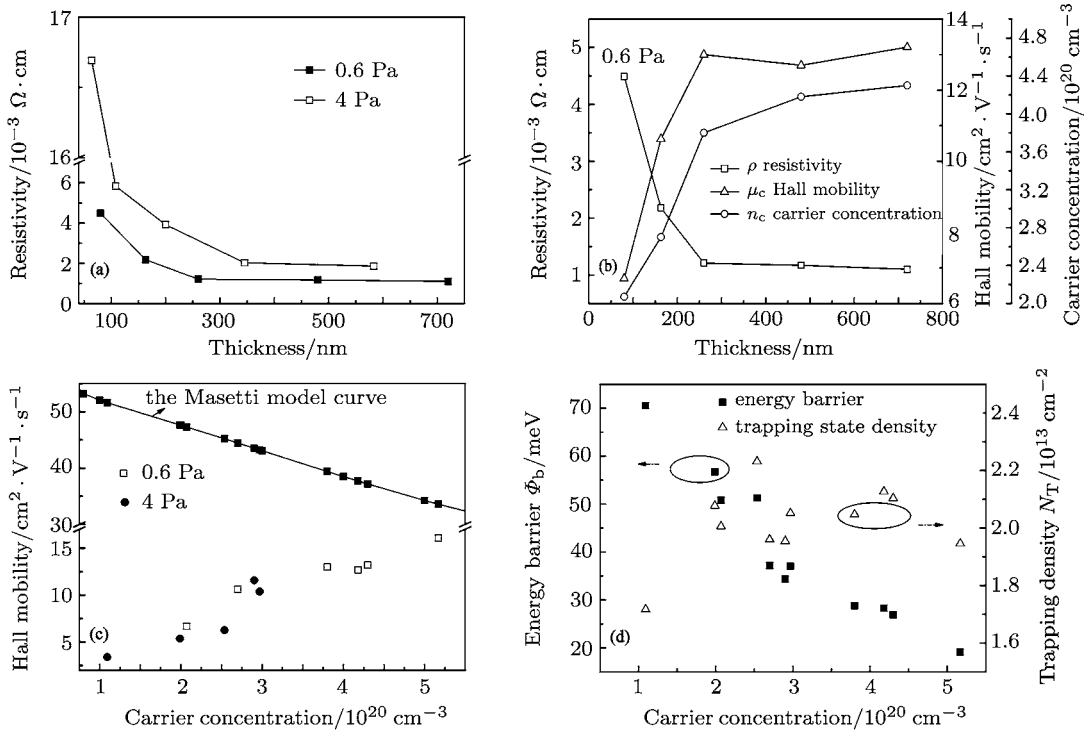
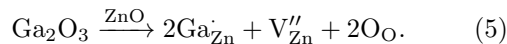
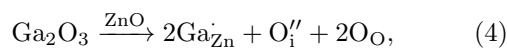


Fig. 3. (a) The dependences of resistivity on film thickness. (b) The resistivity, carrier concentration, and Hall mobility each as a function of film thickness, the films are prepared at 0.6 Pa. (c) All the present data in a plot of Hall mobility versus carrier concentration, and the fitted curve is the Masetti model. (d) The barrier height and the trapping state density each as a function of carrier concentration.

where the dielectric constant ε is 8.5, μ_{in} represents the in-grain mobility (the Masetti upper limit, which is mainly from the ionized impurity scattering), N_T represents the trapping states density, and Φ_b is the barrier height (meV). According to Eqs. (2) and (3), the estimated height of the barrier Φ_b around the grain boundary is shown in Fig. 3(d). As is shown in the figure, the height of the barrier will decrease from 70.5 meV to 19.1 meV with the increase in carrier concentration. The trapping state density N_T is nearly constant, $\sim 1.7 \times 10^{13} \text{ cm}^{-2}$ – $2.2 \times 10^{13} \text{ cm}^{-2}$. The results are similar to those reported previously.^[35–37]

The optical properties of the films grown at 0.6 Pa are investigated by PL spectra at 77 K. The films have different carrier concentrations, which span from $2 \times 10^{20} \text{ cm}^{-3}$ to $4.18 \times 10^{20} \text{ cm}^{-3}$ (the maximal measurement error of n_c is less than 10%), and the film thickness ranges from 80 nm to 480 nm. The PL measurements show that the emission properties vary with the variation in carrier concentration, which is attributed to the film thickness effect. As is well known, the PL spectrum can detect some radiative defects by the optical emission of specific wavelength and the uncertainties usually originate from the overlapped emissions, defect complex, and nonradiative or low-emissive defects. The emission peaks can usually be divided into some categories such as near-band-edge emissions, bandgap tails, and deep-level emissions. As shown in Fig. 4, no fine structures can be detected. Indeed, no fine structures and red shifts of near-band-edge peaks should be expected because of impurities packing close together for heavily doped systems. The dominant emission peaks and relative variations of luminescence intensities can be detected at 2.46 eV and 3.07 eV. For the GZO system, the defect chemical reactions (4) and (5) can be described as



As stated in the discussion given by Janotti and Van de Walle,^[14] the formation energies of zinc interstitials and oxygen interstitials under n-type conditions are high, but the formation energies of zinc vacancies and oxygen vacancies are only 1.5 eV and 3.7 eV, respectively. According to results reported by others,^[38,39] emission peaks of oxygen interstitials and zinc interstitials are at $\sim 2.28 \text{ eV}$ and 3.1 eV , respectively. Therefore, the emission peaks at 2.46 eV and 3.07 eV are

assigned to oxygen vacancies and zinc vacancies, respectively. The suppressed luminescence intensity of zinc vacancies confirms the fact that more Ga atoms will be substituted for zinc vacancies with the increase in film thickness. As demonstrated above, it also leads to the higher carrier concentration. In fact, the anomalous defect concentration distribution along the film growth direction has been observed by using the positron annihilation spectrum by Zubiaga *et al.*^[40] The substitution can occur by the mediations of zinc vacancies due to the lower self-diffusion energy in n-type ZnO.^[14,41] The suppressed luminescence from the thicker film should be attributed to the relaxation of the ZnO host lattice. It results from the increased Ga_{Zn} concentration. Moreover, the luminescence from oxygen vacancies becomes dominant when the thickness is over 260 nm. The results imply that the defect status in the film can be governed greatly by the growth process.

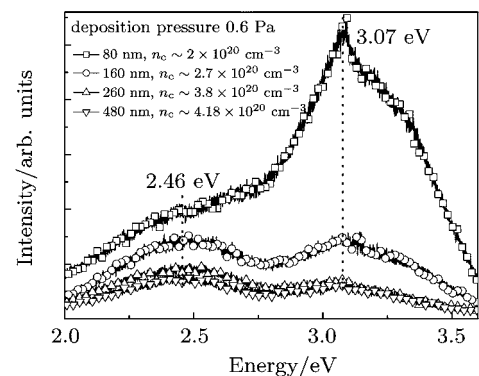


Fig. 4. The PL spectra of the GZO films at 77 K. The films with thicknesses of 80, 160, 260, and 480 nm are prepared at 0.6 Pa.

Figure 5(a) shows that the film has a high transmittance ($> 90\%$) in the visible region. The oscillation from the thicker film is due to the light interference at the interface between the film and the substrate. The inset plot shows the curves of α^2 versus $h\nu$ for the films with the values of carrier concentration (n_c) of $1.09 \times 10^{20} \text{ cm}^{-3}$ and $5.17 \times 10^{20} \text{ cm}^{-3}$, respectively. Here, α represents the absorption coefficient and $h\nu$ represents the photon energy. The linear dependence and the absorption coefficient greater than 10^4 cm^{-1} at the photon energy above the absorption edge obviously indicate that the GZO film is a direct bandgap semiconductor. The optical bandgap is determined by an extrapolation method, at the point where α^2 is zero. Figure 5(b) shows the optical bandgap plotted as a function of the carrier concentration $n_c^{2/3}$ for

all films. An obvious blueshift can be observed with the increase of carrier concentration. The bandgap

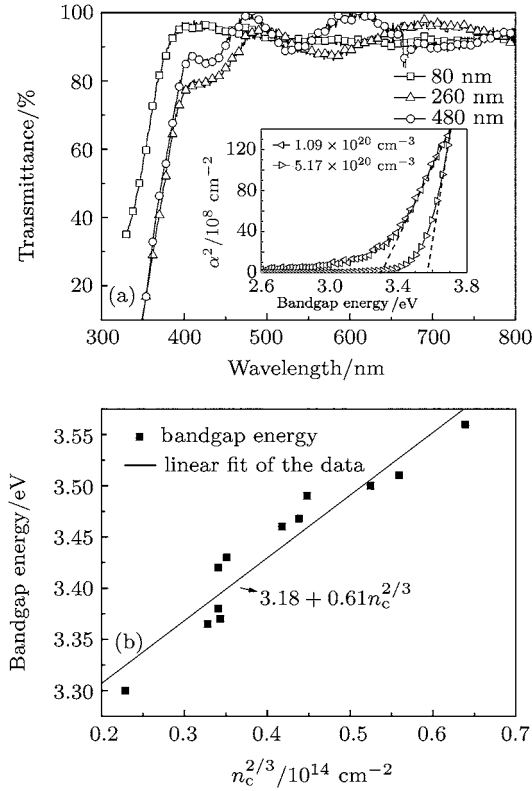


Fig. 5. (a) Optical transmittances of the GZO films with thicknesses of 80, 260, and 480 nm. The inset shows the squared absorption coefficients each plotted as a function of the photon energy with n_c values of $1.09 \times 10^{20} \text{ cm}^{-3}$ and $5.17 \times 10^{20} \text{ cm}^{-3}$, respectively. (b) The optical bandgap plotted as a function of the carrier concentration $n_c^{2/3}$, and the solid line represents the results obtained from the fitted BM model.

is extended from 3.3 eV up to 3.56 eV as the carrier concentration increases from $1.09 \times 10^{20} \text{ cm}^{-3}$ up to $5.17 \times 10^{20} \text{ cm}^{-3}$. In fact, the bandgap will shift due to the Burstein–Moss (B–M) effect only in the degenerate semiconductor.^[42] It means that the carrier concentration n_c should be larger than the conduction band effective density of state N_c for the n-type semiconductor. Usually, the N_c can be expressed as

$$N_c = 2(2\pi m_e^* kT)^{3/2} / h^3. \quad (6)$$

Here, m_e^* represents the effective mass of the electron in the conduction band, which ranges from $0.28m_0$ to $0.5m_0$ as the carrier concentration varies. According to Eq. (6), the evaluated N_c spans from $3.7 \times 10^{18} \text{ cm}^{-3}$ to $8.83 \times 10^{18} \text{ cm}^{-3}$. Thus, the GZO films (the lowest n_c is over $1 \times 10^{20} \text{ cm}^{-3}$) are degenerate for the conduction band and the blueshift will have a remarkable relation with the BM effect. In the

parabolic band approximation, the shift of the optical bandgap in the film can be described as

$$E_g = E_{g0} + \frac{\hbar^2(3\pi^2 n_c)^{2/3}}{2m_{eh}^*}, \quad (7)$$

$$m_{eh}^* = \left[\frac{1}{m_e^*} + \frac{1}{m_h^*} \right]^{-1} \quad (8)$$

with $m_e^* = 0.28m_0$, $m_h^* = 0.59m_0$, Eqs. (7) and (8),^[7] E_g is expressed as $(3.37 + 1.925) \times 10^{-14} n_c^{2/3}$. However, our fitted curve from the experimental data is $(3.18 + 0.61) \times 10^{-14} n_c^{2/3}$. The discrepancy between the derived bandgap of 3.18 eV and the definite bandgap of 3.37 eV can be attributed to the metal–semiconductor transition. Indeed, the metal–semiconductor transition effect should be considered due to the heavy doping. The effect indicates that the valence band will move up by the attraction from the ionized electron gas of dopants, but the conduction band will move down by Urbach band tails due to the merging of the conduction band and the impurity band. As a criterion, the Mott critical concentration is used to evaluate the onset of the bandgap narrowing and can be described as^[43]

$$n_c^{1/3} a^* = K. \quad (9)$$

Here, K is a constant from 0.2 to 0.3 for different materials. In the effective mass approximation, the wavefunction extension of the electron bound to the fixed ion can be expressed as

$$a^* = \varepsilon \hbar^2 / m_e^* \pi e^2 \quad (10)$$

with $m_e^* = 0.28m_0 - 0.5m_0$, Eqs. (9) and (10), the estimated n_c varies from $1.81 \times 10^{18} \text{ cm}^{-3}$ to $3.48 \times 10^{19} \text{ cm}^{-3}$. Therefore, the criterion is satisfied and the transition can occur in the films. The smaller derived bandgap of 3.18 eV is attributed to the metal–semiconductor transition. The other smaller coefficient of 0.61 can arise from the used smaller and constant effective mass of the electron. It will increase with the increase of carrier concentration because of the nonparabolic conduction band effect.

4. Conclusion

We investigate the modulations of structural, electrical, and optical properties of the wurtzite GZO films. The wurtzite structure is observed for all films

with a strong *c*-axis preferential orientation. The substitution of more Ga atoms for Zn atoms with the increase of film thickness is confirmed by the regular position shifts of ZnO (002) peaks toward the higher angle side, the varied carrier concentration, and the suppressed zinc vacancies luminescence from the thicker film. The low Hall mobility is attributed to the grain boundary barrier scattering, and the height of barrier decreases with the increase of carrier concentration. The PL peaks at 2.46 eV and 3.07 eV are attributed to oxygen vacancies and zinc vacancies, respectively. The modulated defect status in the film is also confirmed by the PL spectrum. The obvious blueshift of the optical bandgap can be explained by the BM effect. The bandgap difference between 3.18 eV and 3.37 eV, about 0.2 eV, is attributed to the metal-semiconductor transition.

References

- [1] Noginov M A, Gu L, Livenere J, Zhu G, Pradhan A K, Mundle R, Bahoura M, Barnakov Y A and Podolskiy V A 2011 *Appl. Phys. Lett.* **99** 021101
- [2] Kenji N, Hiromichi O, Kazushige U, Toshio K, Masahiro H and Hideo H 2003 *Science* **300** 1269
- [3] Norris B J, Anderson J and Wager J F 2003 *J. Phys. D: Appl. Phys.* **36** L105
- [4] Cao X, Li X M, Gao X D, Liu X G, Yang C, Yang R and Jin P 2011 *J. Phys. D: Appl. Phys.* **44** 255104
- [5] Özgür Ü, Alivov Y I, Liu C, Teke A, Reshchikov M A, Avrutin V, Dogan S, Cho S J and Morkoç H 2005 *J. Appl. Phys.* **98** 041301
- [6] John F W 2003 *Science* **300** 1245
- [7] Ellmer K 2001 *J. Phys. D: Appl. Phys.* **34** 3097
- [8] Minami T 2000 *MRS Bull.* **25** 38
- [9] Tsukazaki A, Ohtomo A, Onuma T, Ohtani M, Makino T, Sumiya M, Ohtani K, Chichibu S F, Fuke S, Segawa Y, Ohno H, Koinuma H and Kawasaki M 2005 *Nat. Mater.* **4** 42
- [10] Look D C, Leedy K D, Vines L, Svensson B G, Zubiaga A, Tuomisto F, Douth D R and Brillson L J 2011 *Phys. Rev. B* **84** 115202
- [11] Du X L, Mei Z X, Liu Z L, Guo Y, Zhang T C, Hou Y N, Zhang Z, Xue Q K and Kuznetsov A Y 2009 *Adv. Mater.* **21** 4625
- [12] Yan Y F, Zhang S B and Pantelides S T 2001 *Phys. Rev. Lett.* **86** 5723
- [13] Van de Walle C G 2000 *Phys. Rev. Lett.* **85** 1012
- [14] Janotti A and Van de Walle C G 2007 *Phys. Rev. B* **76** 165202
- [15] Bundesmann C, Ashkenov N, Schubert M, Spemann D, Butz T, Kaidashev E M, Lorenz M and Grundmann M 2003 *Appl. Phys. Lett.* **83** 1974
- [16] Hiroyuki F and Michio K 2005 *Phys. Rev. B* **71** 075109
- [17] Karger M and Schilling M 2005 *Phys. Rev. B* **71** 075304
- [18] Jia H, Chen Y H, Liu G H, Liu X L, Yang S Y and Wang Z G 2009 *J. Phys. D: Appl. Phys.* **42** 015415
- [19] Babar R, Deshamukh P R, Deokate R J, Haranath D, Bhosale C H and Rajpure K Y 2008 *J. Phys. D: Appl. Phys.* **41** 135404
- [20] Gregory J E and Xiao D Z 2007 *Thin Solid Films* **515** 7025
- [21] Ilan S, Henryk T and Venkatesh N 2004 *Phys. Rev. B* **69** 245401
- [22] Vlasenko L S, Watkins G D and Helbig R 2005 *Phys. Rev. B* **71** 115205
- [23] Song P K, Watanabe M, Kon M, Mitsui A and Shigesato Y 2002 *Thin Solid Films* **411** 82
- [24] Tsuji T and Hirohashi M 2000 *Appl. Surf. Sci.* **157** 47
- [25] Morito M and Kenichi O 1988 *Appl. Phys. Lett.* **53** 1393
- [26] Hong S K, Jeong S K, Jae W K and Sang Y L 2004 *J. Appl. Phys.* **95** 1246
- [27] Tian Z, Voigt J A and Liu J 2003 *Nat. Mater.* **2** 821
- [28] Agashe C, Kluth O, Hüpkes J, Zastrow U, Rech B and Wuttig M 2004 *J. Appl. Phys.* **95** 1911
- [29] Masetti G, Severi M and Solmi S 1983 *IEEE Trans. Electron Dev.* **ED30** 764
- [30] Tadatsugu M 2008 *Thin Solid Films* **516** 5822
- [31] Takahiro Y, Aki M, Seiichi K, Hisao M, Naoki Y and Tetsuya Y 2007 *Appl. Phys. Lett.* **91** 051915
- [32] Valerie R C and James P S 2008 *Phys. Rev. B* **77** 144111
- [33] Wen W C 2005 *Nat. Mater.* **4** 727
- [34] Yu X Z, Kanazawa N, Onose Y and Kimoto K 2011 *Nat. Mater.* **10** 106
- [35] John Y W S 1975 *J. Appl. Phys.* **46** 5247
- [36] Cornelius S, Vinnichenko M, Shevchenko N, Rogozin A, Kolitsch A and Möller W 2009 *Appl. Phys. Lett.* **94** 042103
- [37] Takaaki T, Shuichi N, Naoki O and Takeshi O 1999 *Jpn. J. Appl. Phys.* **38** 3682
- [38] Cheol H A, Young Y K, Dong C K, Sanjay K M and Hyung K C 2009 *J. Appl. Phys.* **105** 013502
- [39] Xu P S, Sun Y M, Shi C S, Xu F Q and Pan H B 2003 *Nucl. Instrum. Methods B* **199** 286
- [40] Zubiaga A, Garcia J A, Plazaola F, Tuomisto F, Saarinen K, Zuniga P J and Munoz S V 2006 *J. Appl. Phys.* **99** 053516
- [41] Gregory W T, Jules L R and Thomas O M 2000 *J. Appl. Phys.* **87** 117
- [42] Elias B 1954 *Phys. Rev.* **93** 632
- [43] Mott N F 1961 *Philos. Mag.* **6** 287